Mechanism of Assembly of the Tyrosyl Radical–Diiron(III) Cofactor of *E. Coli* Ribonucleotide Reductase. 1. Mössbauer Characterization of the Diferric Radical Precursor

Natarajan Ravi,[†,⊥] J. Martin Bollinger, Jr.,[§,∥] Boi Hanh Huynh*[,†] Dale E. Edmondson,*[,‡] and JoAnne Stubbe*[,§]

Contribution from the Departments of Physics and Biochemistry, Emory University, Atlanta, Georgia 30322, and the Departments of Chemistry and Biology, Massachusetts Institute of Technology, Cambridge, Massachusetts 02139

Received January 13, 1994[⊗]

Abstract: The R2 subunit of *Escherichia coli* ribonucleotide reductase (RNR) contains a cofactor which consists of a stable tyrosyl radical (•Y122) adjacent to a μ-oxo-bridged diiron(III) cluster. This cofactor assembles spontaneously when apo R2 is treated with Fe^{2+} and O_2. By using rapid kinetic techniques, two kinetically competent intermediates in this assembly process were recently identified (Bollinger, J. M., Jr. et al. *Science* **1991**, *253*, 292–298). One of the intermediates is a paramagnetic iron species. By using the rapid freeze–quench technique and a mutant R2 subunit in which Y122 is replaced with F, 1 equiv of this intermediate per R2 subunit can be trapped. Previous electron paramagnetic resonance (EPR) and Mössbauer studies suggested that this species is a spin coupled system involving two high-spin ferric ions and a free radical (a "diferric radical species") (Bollinger, J. M., Jr. et al. *J. Am. Chem. Soc.* **1991**, *113*, 6289–6291). In the present study, Mössbauer spectra have been recorded over a wide range of applied fields (60 mT–8 T), and detailed analysis of the Mössbauer data consolidates the initial finding. The observed isomer shifts (0.55 mm/s for iron site 1 and 0.36 mm/s for site 2) and quadrupole splittings ($\sim$1 mm/s) are typical for high-spin ferric species. The magnetic hyperfine coupling tensors, A, for the two iron sites are relatively isotropic (within 20%), a feature which is unique to high-spin Fe(III). By using a simple three-spin coupling model ($S_1 = {}^5/_2$ and $S_2 = {}^5/_2$ for the two iron sites, and $S_3 = {}^1/_2$ for the radical), both the signs and magnitudes of the observed A values for the iron sites ($A_1/g_n\beta_n = -52.5$ T and $A_2/g_n\beta_n = +24$ T) can be explained with an intrinsic A value that is consistent with high-spin Fe(III). The asymmetry in the A values for the two iron sites is a result of the spin orientations: the spin of the radical is parallel to that of the negative-A-value Fe site and antiparallel to that of the positive-A-value Fe site. Since it has been suggested on the basis of functional analogy with heme-iron-dependent peroxidases that generation of •Y122 in RNR-R2 may involve a high-valent iron–oxo intermediate, the possibility that this paramagnetic iron species contains Fe(IV) has also been carefully examined. Both the EPR and the Mössbauer data are incompatible with such a possibility.

Introduction

Ribonucleotide reductases (RNRs) catayze the first committed and rate limiting step of DNA biosynthesis, the reduction of nucleotides to 2′-deoxynucleotides.[1-4] The RNRs from *E. coli* and mammals, as well as those encoded by several medically important viruses (e.g. herpes simplex, and rabies), share a common quaternary structural motif and metallocofactor requirement. Each is composed of two homodimeric subunits, which are both required for catalytic activity. The larger subunit, designated R1, contains the following in each of its protomers: (1) binding sites for the nucleoside diphosphate substrates and the nucleoside and deoxynucleoside triphosphate allosteric effectors and (2) multiple cysteine residues which cycle between sulfhydryl and disulfide forms to deliver reducing equivalents to the substrate. The smaller subunit, R2, contains the enzyme's catalytically essential, complex metallocofactor, a μ-oxo-bridged diiron(III) cluster in close proximity to a stable tyrosyl free radical (Figure 1[5-7]). Mössbauer data[8] and the recently reported crystal structure[5] indicate that each monomer of R2 contains a diiron cluster. However, as isolated from overproducing strains of *E. coli* following addition of excess Fe^{2+} and ascorbate to crude extracts, R2 typically contains only 2.8–3.2 equiv of Fe and 1.0–1.3 equiv of tyrosyl radical per dimeric subunit.[9] The less-than-theoretical cofactor stoichiometry has not yet been satisfactorily explained.

Evidence indicates that the first step in the catalytic mechanism of *E. coli* RNR (indeed, of all RNRs thus far investigated) is homolytic scission of the 3′-C–H bond of the nucleotide substrate.[3,10,11] It has been proposed that this step is effected by a protein-derived free radical.[3,12] Until recent X-ray diffraction

* Authors to whom correspondence should be sent.
† Department of Physics, Emory University.
‖ Massachusetts Institute of Technology.
‡ Department of Biochemistry, Emory University.
⊥ Present address: Department of Chemistry, Carnegie Mellon University, Pittsburgh, PA 15213.
§ Present address: Department of Biological Chemistry and Molecular Pharmacology, Harvard Medical School, Boston, MA 02115.
⊗ Abstract published in *Advance ACS Abstracts*, August 15, 1994.

(1) Fontecave, M.; Nordlund, P.; Eklund, H.; Reichard, P. *Adv. Enzymol. Relat. Areas Mol. Biol.* **1992**, *65*, 147–183.
(2) Eriksson, S.; Sjöberg, B.-M. In *Allosteric Enzymes*; Hervé, G., Ed.; CRC Press: Boca Raton, FL, 1989; pp 189–215.
(3) Stubbe, J. *Adv. Enzymol. Relat. Areas Mol. Biol.* **1990**, *63*, 349–419.
(4) Lammers, M.; Follmann, H. *Struct. Bonding (Berlin)* **1983**, *54*, 27–91.
(5) Nordlund, P.; Sjöberg, B. M.; Eklund, H. *Nature* **1990**, *345*, 593–598.
(6) Norlund, P.; Eklund, H. *J. Mol. Biol.* **1993**, *232*, 123–164.
(7) In order to clarify comparison of the crystallographic data of Nordlund *et al.*[5,6] with our Mössbauer data, the designations Fe1 and Fe2 used by Norlund *et al.* have been changed to Fe_A and Fe_B, respectively.
(8) Lynch, J. B.; Juarez-Garcia, C.; Münck, E.; Que, L., Jr. *J. Biol. Chem.* **1989**, *264*, 8091–8096.
(9) Bollinger, J. M., Jr. Ph.D. Thesis, Massachusetts Institute of Technology, 1993. Several methods of extraction of Fe from R2 (including the method of Lynch *et al.*[8]) and several methods for quantitation of the extracted Fe (including atomic absorption and plasma emission[8] spectroscopies, and a colometric method[55,57]) were compared. In all cases the Fe/R2 ratio was found to be 2.8–3.2, assuming ϵ_{280} of R2 = 131 mM^{-1} cm^{-1}.[86]
(10) Stubbe, J.; Ackles, D. *J. Biol. Chem.* **1980**, *255*, 8027–8030.
(11) Stubbe, J.; Ackles, D.; Segal, R.; Blakley, R. L. *J. Biol. Chem.* **1981**, *256*, 4843–4846.
(12) Mao, S. S.; Holler, T. P.; Yu, G.-X.; Bollinger, J. M., Jr.; Booker, S.; Johnston, M. I.; Stubbe, J. *Biochemistry* **1992**, *31*, 9733–9743.

0002-7863/94/1516-8007$04.50/0

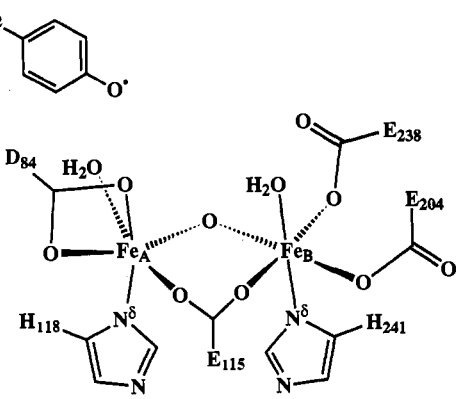

Figure 1. Schematic depiction of the R2 cofactor (adapted[7] from ref 5).

data revealed that the cofactor of *E. coli* R2 is located in the interior of the helical protein (approximately 10 Å from the proposed R1-binding surface),[5,6] the tyrosyl radical was considered the obvious candidate for the 3′-H abstracting species. Because it is unlikely that a large-scale conformational change brings the tyrosyl radical into bonding distance of the 3′-H of the substrate[13] (which is bound in R1), we[12,14,15] and others[6,16] have proposed that the R2 radical participates indirectly in 3′-C–H bond homolysis by generating (via long distance electron transfer) a reactive radical on the R1 subunit. This hypothesis underscores the likely functional importance of electron transfer to and from the cofactor in R2.

As originally shown by Reichard and co-workers,[17] assembly of the R2 cofactor can occur spontaneously *in vitro*. Treatment of native *E. coli* R2 with a chelator and an appropriate denaturant (1 M imidazole) effects removal of the iron cluster and concomitant reduction of the tyrosyl radical, producing the catalytically inactive apo R2. Upon addition of Fe^{2+} and O_2 to apo R2, the native protein is rapidly regenerated. Thus, R2 directs the assembly of its iron–radical cofactor. In this reconstitution reaction, the diferrous form of the iron cluster reductively activates O_2 to effect the one-electron oxidation of tyrosine 122 (Y122).[18] In the process the μ-oxodiferric cluster is generated.

The reaction of O_2 at a diiron(II) center is not unique to R2.[19–25] Other proteins known or believed to share this functional motif include hemerythrin (the O_2-carrying protein of certain marine invertebrates), methane monooxygenase from methanotrophic bacteria, and stearoyl-CoA Δ9 desaturase from yeast and plants.[26] For each of these diiron proteins, the chemical outcome of the O_2 reaction is distinct: in hemerythrin O_2 is reversibly bound in a hydroperoxodiferric complex;[27–29] in methane monooxygenase

Scheme 1. Mechanism Proposed in Our Previous Work[37] for Assembly of the R2 Cofactor[a]

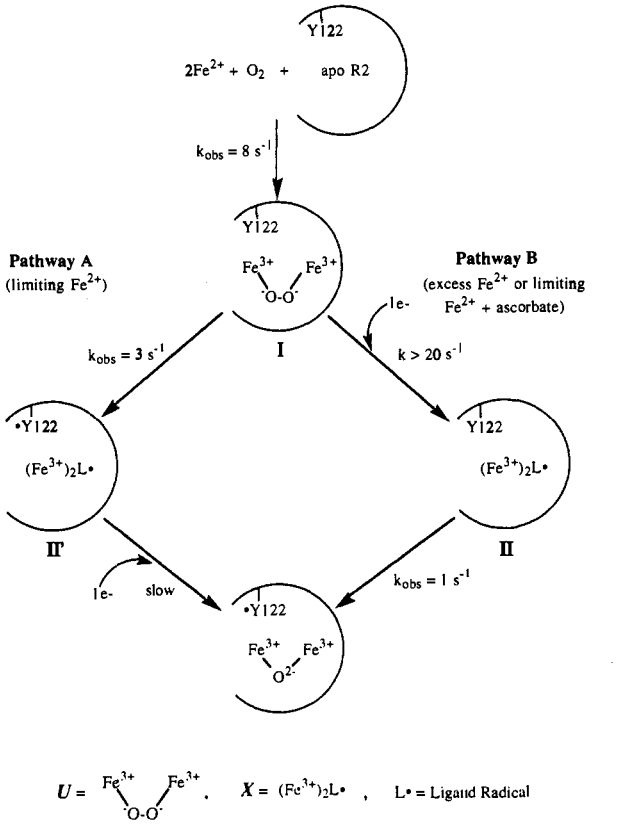

[a] Adapted from ref 37.

O_2 is activated for the two-electron oxidation (hydroxylation) of an unactivated hydrocarbon;[30–35] in stearoyl-CoA Δ-9 desaturase O_2 is activated for the unconjugated dehydrogenation of a stearoyl thioester;[26] and in R2, O_2 is activated for the one-electron oxidation of an endogenous tyrosine residue.[1,17,36–37] An objective which is central to the study of these diiron proteins is to identify structural and electronic features of the iron clusters and their protein chelators which allow similar centers to mediate very different reactions with O_2. A meaningful understanding of structure–function relationships in these proteins clearly requires knowledge of both structure and chemical mechanism.

Because of the importance of the tyrosyl radical–diiron(III) cofactor to the function of RNR, and because of the general biochemical significance of reactions between O_2 and diiron clusters, we recently began to investigate the mechanism by which *E. coli* R2 self-assembles its cofactor from Fe^{2+} and O_2. Rapid kinetic/spectroscopic methods, including stopped-flow absorption (SF-Abs), rapid freeze-quench EPR (RFQ-EPR), and rapid freeze-quench Mössbauer (RFQ-Möss) spectroscopies, were used in conjunction with site-directed mutagenesis to probe the reconstitution mechanism.[37,38] Evidence was obtained for the accumulation of two intermediate species (Scheme 1).[37] The

(13) Ehrenberg, A. *Chem. Scr.* **1988**, *28A*, 27–31.
(14) Mao, S. S.; Yu, G.-X.; Chalfoun, D.; Stubbe, J. *Biochemistry* **1992**, *31*, 9752–9759.
(15) Stubbe, J. *J. Biol. Chem.* **1990**, *265*, 5329–5332.
(16) Nordlund, P. Ph.D. Thesis, Swedish University of Agricultural Sciences, 1990.
(17) Atkin, C. L.; Thelander, L.; Reichard, P.; Lang, G. *J. Biol. Chem.* **1973**, *248*, 7464–7472.
(18) Larsson, A.; Sjöberg, B.-M. *EMBO J.* **1986**, *5*, 2037–2040.
(19) Feig, A. L.; Lippard, S. J. *Chem. Rev.* **1994**, in press.
(20) Stubbe, J. *Curr. Opin. Struct. Biol.* **1991**, *1*, 788–795.
(21) Que, L., Jr.; True, A. E. *Prog. Inorg. Chem. Bioinorg. Chem.* **1990**, *38*, 97–200.
(22) Vincent, J. B.; Oliver-Lilley, G. L.; Averill, B. A. *Chem. Rev.* **1990**, *90*, 1447–1467.
(23) Kurtz, D. M., Jr. *Chem. Rev.* **1990**, *90*, 585–606.
(24) Sanders-Loehr, J. In *Iron Carriers and Iron Proteins*; Loehr, T. M., Ed.; VHC Publishers Inc., 1989; pp 375–466.
(25) Lippard, S. J. *Angew. Chem., Int. Ed. Engl.* **1988**, *27*, 344–361.
(26) Fox, B. G.; Shanklin, J.; Somerville, C.; Münck, E. *Proc. Natl. Acad. Sci. U.S.A.* **1993**, *90*, 2486–2490.
(27) Shiemke, A. K.; Loehr, T. M.; Sanders-Loehr, J. *J. Am. Chem. Soc.* **1984**, *106*, 4951–4956.
(28) Stenkamp, R. E.; Sieker, L. C.; Jensen, L. H.; McCallum, J. D.; Sanders-Loehr, J. *Proc. Natl. Acad. Sci. U.S.A.* **1985**, *82*, 713–716.
(29) Shiemke, A. K.; Loehr, T. M.; Sanders-Loehr, J. *J. Am. Chem. Soc.* **1986**, *108*, 2437–2443.
(30) Dalton, H. *Adv. Appl. Microbiol.* **1980**, *26*, 71–87.
(31) Woodland, M. P.; Dalton, H. *J. Biol. Chem.* **1984**, *259*, 53–59.
(32) Green, J.; Dalton, H. *J. Biol. Chem.* **1985**, *260*, 15795–15801.
(33) Fox, B. G.; Froland, W. A.; Dege, J. E.; Lipscomb, J. D. *J. Biol. Chem.* **1989**, *264*, 10023–10033.
(34) Liu, K. E.; Johnson, C. C.; Newcomb, M.; Lippard, S. J. *J. Am. Chem. Soc.* **1993**, *115*, 939–947.
(35) Rosenzweig, A. C.; Frederick, C. A.; Lippard, S. J.; Nordlund, P. *Nature* **1993**, *366*, 537–543.
(36) Sahlin, M.; Gräslund, A.; Petersson, L.; Ehrenberg, A.; Sjöberg, B.-M. *Biochemistry* **1989**, *28*, 2618–2625.
(37) Bollinger, J. M., Jr.; Edmondson, D. E.; Huynh, B. H.; Filley, J.; Norton, J. R.; Stubbe, J. *Science* **1991**, *253*, 292–298.
(38) Bollinger, J. M., Jr.; Stubbe, J.; Huynh, B. H.; Edmondson, D. E. *J. Am. Chem. Soc.* **1991**, *113*, 6289–6291.

first species (then designated *U*[39]) accumulates only when the reaction is carried out with limiting Fe^{2+} in the absence of additional reductant (e.g. ascorbate) and is characterized by a broad absorption band centered at 560 nm. On the basis of this feature, which is similar to that of a model complex prepared by Que and co-workers,[40] and on the basis of additional chemical precedent,[41] the 560 nm absorbing species was postulated to be a μ-peroxodiferric cluster.[37] The second intermediate species, *X*, which accumulates under all reaction conditions examined, was proposed on the basis of its EPR and Mössbauer spectra to consist of two high-spin ferric ions coupled to a ligand radical (the diferric radical species).[38] Preliminary kinetic data were interpreted as evidence that each of the proposed intermediate iron clusters can generate •Y122. In consideration of these kinetic and spectroscopic data and the fact that an "extra" electron, in addition to the three obtained in oxidization of the diferrous cluster and Y122, is required in the reaction to balance the four-electron reduction of O_2,[37,42–44] the mechanism shown in Scheme 1 was proposed.[37] The key features of this hypothesis are (1) the partition of the reaction between pathways A and B, with the partition ratio depending on the availability of the extra reducing equivalent, and (2) the generation of •Y122 by a different intermediate iron cluster in each pathway (*U* in pathway A and *X* in pathway B).

In the work that is described in this paper and the two that accompany it, we have extended our study of the R2 cofactor assembly reaction in two ways. First, we have used the three independent and complementary methods employed in our earlier work, SF-Abs, RFQ-EPR, and RFQ-Möss spectroscopies, to thoroughly examine the kinetics of the cofactor assembly under a limited set of reaction conditions. In agreement with our previous work, the kinetic and spectroscopic characteristics of the reaction have been observed by each method to depend markedly on the initial ratio of Fe^{2+} to R2 (which determines the availability of the extra electron). Results from the reaction of apo R2 with excess Fe^{2+} (Fe^{2+}/R2 = 5) are reported in paper 2 of this series.[42] The data are consistent with the proposal of Scheme 1 that the intermediate *X* generates •Y122 and is the direct precursor to the product diferric cluster under these reaction conditions. Rate constants determined by the three different methods show quantitative agreement, illustrating the complementarity of the approaches. Results from the reaction of apo R2 with limiting Fe^{2+} (Fe^{2+}/R2 = 2.0–2.4), which are presented in paper 3,[45] also agree with Scheme 1, inasmuch as they are consistent with the proposal that the 560 nm absorbing species generates •Y122 under these conditions. An important discrepancy with Scheme 1 arises, however, when the SF-Abs and RFQ-Möss kinetic data are compared. The results suggest that the 560 nm absorption band is not associated with an iron species and, therefore, most likely arises from a modification of the protein. On the basis of this result and precedent from the chemical[46–48] and biochemical literature,[49] we tentatively propose that the absorbing species is a tryptophen cation radical. The possible identity of the W residue that is oxidized and implications with respect to the catalytic mechanisms of RNR and other dinuclear iron proteins are discussed.

Also as an extension of our previous study,[37,38] we have more thoroughly characterized the intermediate iron cluster, *X*, by Mössbauer and EPR spectroscopies. The spectral data, which are reported in this paper, provide strong support for our previous structural assignment: the observed parameters are consistent with a model for *X* involving two high-spin ferric ions and a free radical. As it has repeatedly been proposed that •Y122 is generated by an Fe(IV)-containing intermediate,[50–53] the possibility that *X* contains Fe(IV) has been carefully examined, and the data have been shown to be inconsistent with such a possibility. Thus, the results of this and the following paper[42] suggest, in contrast to what has been proposed in the literature,[50–53] that the •Y122-generating intermediate in the case of the kinetically simple excess Fe^{2+} reaction does not contain Fe(IV). Furthermore, analysis presented herein sheds light on the possible identities of the radical component in the key diferric radical precursor to the R2 cofactor.

Materials and Methods

Preparation of Apo R2-Y122F. A site-directed mutant R2 subunit, R2-Y122F,[18,37] was used in this study, because as much as 1 equiv of *X* per subunit can be trapped when Y122 is replaced with the less easily oxidized F.[38] Preparation of apo R2-Y122F is described in the supplementary material to paper 2 of this series.[42]

Preparation of the Rapid Freeze–Quench Mössbauer Samples. The rapid freeze-quench instrument consists of an Update Instruments (Madison, WI) Ram Unit, a Model 705A computer controller, and a home-built quenching bath. The bath holds approximately 8 L of isopentane which is cooled by liquid nitrogen and maintained at −140 °C with a Bayley Instruments Co. (Danville, CA) precision temperature controller. The procedure for preparing Mössbauer samples is similar to that described previously for the preparation of EPR samples.[54] The method involves mixing two reactants rapidly and efficiently through a mixing chamber, allowing the reaction to proceed for the length of time required for it to traverse an aging hose of appropriate volume, freeze-quenching the reaction mixture by squirting it into the quenching bath containing isopentane at −140 °C, and packing the frozen ice crystals of the reaction mixture through a sample-collecting apparatus into a receptacle appropriate for spectroscopic analysis. A schematic drawing of the apparatus is shown in Figure 2. The apparatus was assembled, placed in its holder, filled with isopentane, inserted into the cold isopentane quenching bath, and allowed to reach thermal equilibrium with the bath (−140 °C). The spray nozzle at the end of the aging hose was held less than 1 cm above the level of isopentane in the glass funnel, and the reactants were mixed and sprayed into the cold isopentane by actuation of the ram drive. Approximately 500 μL of reaction mixture was required to generate a satisfactory sample. The velocity of the ram drive was 1 cm/s, which produced ice crystals coarse enough to settle properly. Finer crystals produced with faster ram velocities tended to float during packing, resulting in loss of sample. The crystals were allowed to settle for approximately 1 min and were then packed into the Mössbauer cell. With the packer still pressing on the sample, the entire sampling apparatus was

(39) The 560 nm absorbing species was proposed in ref 37 to be a μ-peroxodiferric cluster and was therein designated *U*. For reasons which will become apparent, the absorbing species will not be referred to as *U* in this and the accompanying papers.[42,45] In general, we have amended our nomenclature such that the postulated intermediate states of R2 are now designated as **I**, **II**, and **II′**. The diferric radical species, shown as a component of both **II** and **II′**, is still designated as *X*.

(40) Menage, S.; Brennan, B. A.; Juarez-Garcia, C.; Münck, E.; Lawrence Que, J. *J. Am. Chem. Soc.* **1990**, *112*, 6423–6425.

(41) Brennan, B. A.; Chen, Q.; Juarez-Garcia, C.; True, A. E.; O'Connor, C. J.; Que, L., Jr. *Inorg. Chem.* **1991**, *30*, 1937–1943 and references cited therein.

(42) Part 2: Bollinger, J. M., Jr.; Tong, W. H.; Ravi, N.; Huynh, B. H.; Edmondson, D. E.; Stubbe, J. *J. Am. Chem. Soc.*, second of three papers in this issue.

(43) Elgren, T. E.; Lynch, J. B.; Juarez-Garcia, C.; Münck, E.; Sjöberg, B.-M.; Que, L., Jr. *J. Biol. Chem.* **1991**, *266*, 19265–19268.

(44) Ochiai, E.-I.; Mann, G. J.; Gräslund, A.; Thelander, L. *J. Biol. Chem.* **1990**, *265*, 15758–15761.

(45) Part 3: Bollinger, J. M., Jr.; Tong, W. H.; Ravi, N.; Huynh, B. H.; Edmondson, D. E.; Stubbe, J. *J. Am. Chem. Soc.*, third of three papers in this issue.

(46) Solar, S.; Getoff, N.; Surdhar, P. S.; Armstrong, D. A.; Singh, A. *J. Phys. Chem.* **1991**, *95*, 3639–3643 and references cited therein.

(47) Jovanovic, S. V.; Simic, M. G. *J. Free Radicals Biol. Med.* **1985**, *1*, 125–129.

(48) Posener, M. L.; Adams, G. E.; Wardman, P. *J. Chem. Soc., Faraday Trans. 1* **1976**, *72*, 2231–2239.

(49) Houseman, A. L. P.; Doan, P. E.; Goodin, D. B.; Hoffman, B. M. *Biochemistry* **1993**, *32*, 4430–4443 and references cited therein.

(50) Que, L., Jr. *Science* **1991**, *253*, 273.

(51) Fontecave, M.; Gerez, C.; Atta, M.; Jeunet, A. *Biochem. Biophys. Res. Commun.* **1990**, *168*, 659–664.

(52) Sahlin, M.; Sjöberg, B.-M.; Backes, G.; Loehr, T.; Sanders-Loehr, J. *Biochem. Biophys. Res. Commun.* **1990**, *167*, 813–818.

(53) Ling, J.; Sahlin, M.; Sjöberg, B.-M.; Loehr, T. M.; Sanders-Loehr, J. *J. Biol. Chem.* **1994**, *269*, 5595–5601.

(54) Ballou, D. P. *Methods Enzymol.* **1978**, *54*, 85–93.

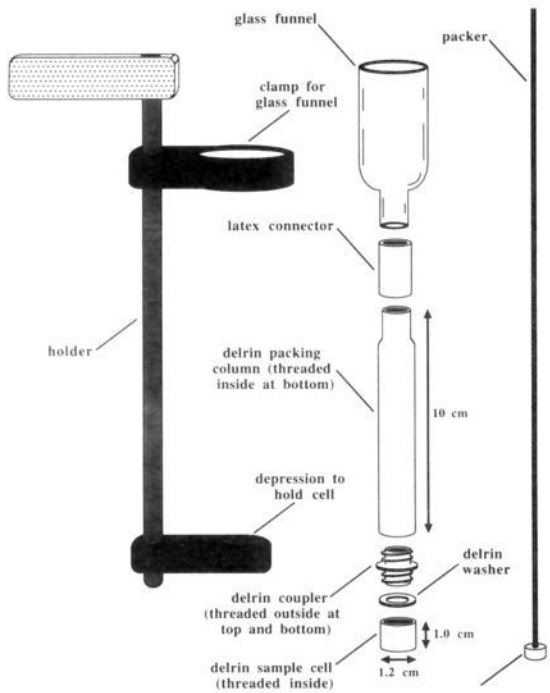

Figure 2. Schematic drawing of the sample-collecting apparatus used to prepare RFQ-Möss samples.

removed from the bath, and the bottom part of the apparatus (including the Mössbauer cell) was submerged as rapidly as possible into a slush of partially frozen isopentane contained in a wide-mouth (13 cm in diameter and 8 cm in height) stainless-steel dewar. Next, the glass funnel with the latex connector, the delrin packing column with the coupler, and the packer were removed from the sample cell in the sequence described. A hex-nut style, threaded delrin sample cap (not shown) was then attached to the end ot a hex-key wrench and precooled in the isopentane slush. The sample cell was grasped with pre-cooled tweezers and the cap was screwed into the cell. When the cap was tight, the sample was removed from the slush, detached from the hex key, briefly wiped free of isopentane, and dropped into liquid nitrogen. For preparation of the Mössbauer samples used in this study, 1.5 mM apo R2-Y122F in O_2-saturated 100 mM HEPES buffered at pH 7.7 was mixed with an equal volume of an O_2-saturated $^{57}Fe^{2+}$ stock solution (described below). The temperature of the reconstitution reaction was maintained at (5 ± 1) °C by submerging the drive syringes, which contained the two reactants, and the aging hose in an ice–water bath at the desired temperature. The reaction was quenched after 0.31 s.

The $^{57}Fe^{2+}$ stock solution was prepared by addition of 150 μL of O_2-free 1 M H_2SO_4 to a 5.3 mg nugget of ^{57}Fe metal (95% plus enrichment, Advanced Materials and Technology, New York, NY). The mixture was incubated at ambient temperature in an anaerobic chamber for 4 days. After this time, the liquid was taken off and diluted to 7.5 mL with O_2-free H_2O. This stock was assayed for [Fe^{2+}] using ferrozine[55-57] and was found to be 6.2 mM in Fe^{2+}, indicating that about half of the iron metal had dissolved. In order to obtain the desired Fe^{2+}/apo R2 ratio, a 2 mL aliquot of this stock solution was diluted with 0.76 mL of H_2O and 28 μL of 0.5 M sodium ascorbate in H_2O. This final stock solution was filtered through a 0.22 μm filter and assayed for [Fe^{2+}]. It was found to be 4.5 mM in Fe^{2+}.

Mössbauer Spectroscopy. Mössbauer spectra were recorded either on a weak-field Mössbauer spectrometer equipped with a Janis 8DT variable-temperature cryostat or on a strong-field Mössbauer spectrometer equipped with a Janis 12 CNDT/SC SuperVaritemp cryostat containing an 8 T superconducting magnet. Both spectrometers were operated in a constant acceleration mode in a transmission grometry. The zero velocity of the Mössbauer spectra refers to the centroid of the room temperature spectrum of a metallic iron foil.

(55) Salowe, S. P. Ph.D. Thesis, University of Wisconsin, 1987.
(56) Stookey, L. L. *Anal. Chem.* **1970**, *42*, 779–781.
(57) Massey, V. *J. Biol. Chem.* **1957**, *229*, 763–770.

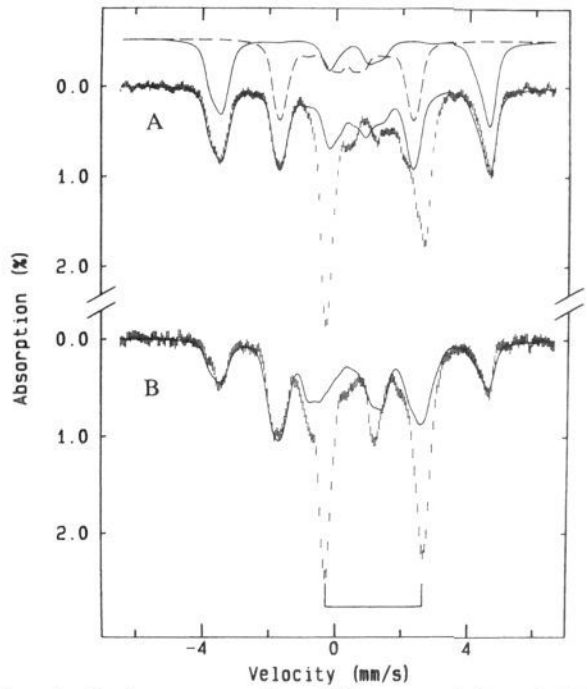

Figure 3. Mössbauer spectra of a rapid freeze-quenched sample (310 ms) from the reaction of apo R2-Y122F with 3 equiv of Fe^{2+}, O_2, and ascorbate. The spectra were recorded at 4.2 K with a magnetic field of 60 mT applied (A) parallel or (B) perpendicular to the γ-beam. The *solid lines* plotted through the experimental data are simulated spectra of *X* generated by using the parameters listed in Table 1. They are normalized to 70% of the total absorption. Theoretical parallel field spectra of the individual iron sites are shown at the top of the figure: site 1 (—); site 2 (– – –). The bracket indicates the positions of the ferrous quadrupole doublet.

Results

For this study, we made use of a site-directed mutant of R2 in which the oxidizable Y122 is replaced with F (R2-Y122F).[18,37] The diferric radical species can be trapped in high yields (1 equiv/subunit) in this mutant protein, and the spectroscopic properties of *X* generated in R2-Y122F are identical with those of the intermediate generated in wild type R2.[38] Figure 3 shows Mössbauer spectra of a freeze-quenched sample (0.31 s) from the reaction of apo R2-Y122F with Fe^{2+} (3 equiv), O_2, and ascorbate. The spectra were recorded at 4.2 K with a magnetic field of 60 mT applied parallel (Figure 3A) or perpendicular (Figure 3B) to the γ-beam. The spectra show a central quadrupole doublet which accounts for (32 ± 3)% of the total absorption, and a paramagnetic component which accounts for (68 ± 3)%. The doublet exhibits parameters (ΔE_Q = 3.20 mm/s and δ = 1.30 mm/s) consistent with either the diferrous cluster of R2 or high-spin ferrous ions in HEPES.[8] The paramagnetic component is attributed to the diferric radical intermediate on the basis of previously reported EPR data taken on a duplicate sample. The EPR sample showed a nearly isotropic signal at g = 2.0 with magnetic hyperfine structure resulting from the unpaired electron interacting with two ^{57}Fe nucleii (nuclear spin $I = {}^1/_2$).[38] In order to further characterize the diferric radical intermediate, Mössbauer spectra in strong applied fields were recorded (Figure 4). These spectra confirm our earlier analysis that the paramagnetic species is composed of two components of equal intensity, which correspond to two distinct iron sites (top of Figures 3 and 4). Moreover, the strong-field spectra (Figure 4) indicate that the spins of the iron sites are coupled in an antiparallel manner, since the total magnetic splitting is seen to decrease for site 1 and increase for site 2 with increasing applied field strength. In the weak-field spectrum (Figure 3) the highest energy line of site 2 overlaps with that of the ferrous doublet, which introduced

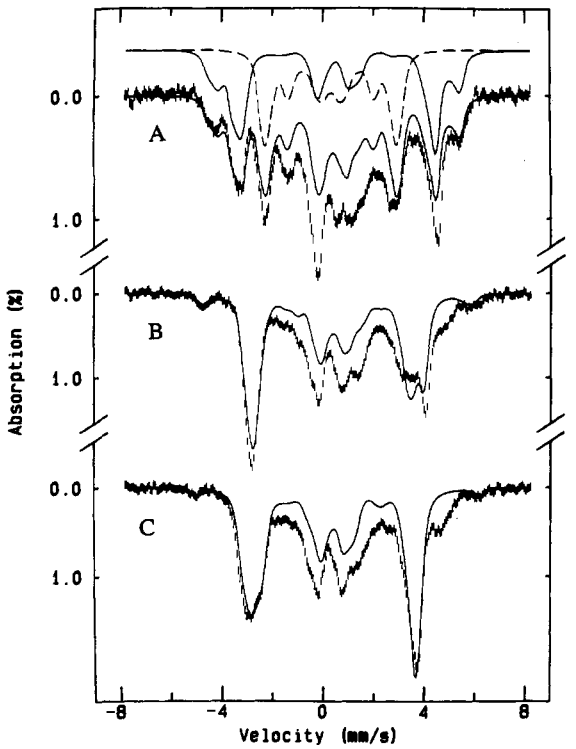

Figure 4. Mössbauer spectra of the sample from Figure 3 recorded in strong applied fields. The spectra were acquired at 4.2 K with parallel applied fields of (A) 3, (B) 6, and (C) 8 T. The *solid lines* plotted through the experimental data are theoretical spectra of X based on the parameters listed in Table 1. They are normalized to 70% of the total absorption. Theoretical spectra of the individual iron sites for the 3 T parallel field are shown at the top of the figure: site 1 (—); site 2 (- - -).

uncertainty in our earlier analysis of site 2.[38] Since the magnetic saturation behavior of the diferric radical intermediate ($S = {}^1/_2$) differs from that of the ferrous ions, in the presence of a strong field the spectrum of site 2 becomes resolved from the ferrous ion spectrum. By carefully examining the pattern of the paramagnetic component as a function of the applied field, the absorption spectrum originating from iron site 2 was better defined. In order to obtain characteristic parameters for the diferric radical intermediate, the data were analyzed according to the following spin Hamiltonian

$$\mathbf{H} = \beta\vec{S}\cdot\tilde{g}\cdot\vec{H} + \sum_{i=1}^{2}\vec{S}\cdot\tilde{A}_i\cdot\vec{I}_i + \sum_{i=1}^{2}\frac{eQV_{zzi}}{4}\left[I_{zi}^2 - I_i(I_i+1)/3 + \frac{\eta}{3}(I_{xi}^2 - I_{yi}^2)\right] - \sum_{i=1}^{2}g_n\beta_n\vec{H}\cdot\vec{I}_i \quad (1)$$

where S is the system spin (1/2) and i designates the iron sites (1 or 2). By systematically varying the parameters, several hundred theoretical spectra were generated, and the simulations were compared with the experimental data. The parameter set listed in Table 1 yields theoretical simulations that are in best agreement with the experimental data. The *solid lines* in Figures 3 and 4, which are overlayed with the experimental spectra, are simulations based on these parameters. It is important to note that, even though the spectral component of iron site 2 of the diferric radical intermediate overlaps partially with the ferrous spectral component, data recorded over a wide range of experimental conditions exhibit enough resolution to allow for reliable determination of its parameters. Since the ferrous component and the iron site 1 component are well-defined in the 60 mT spectra (Figure 3), their isomer shifts can be determined with good accuracy. The isomer shift of iron site 2 can then be derived from the center of gravity of the whole spectrum by using the isomer shifts obtained for the ferrous component and iron site 1. Using δ(ferrous component) = 1.26–1.30 mm/s and δ(iron site 1) = 0.5–0.55 mm/s, δ(iron site 2) was estimated to be within the 0.35–0.41 mm/s range. With these isomer shift values, accurate simulation of the spectra requires relatively isotropic A values (within 20%) and small values of ΔE_Q (0.5–1.6 mm/s) for both iron sites. Analysis with a smaller δ for iron site 2 has also been explored, and the findings are discussed below.

Table 1. Mössbauer Parameters for the Diferric Radical Species

	iron site 1	iron site 2
$A/g_n\beta_n$ (T)[a]	−52.5	+24.0
δ (mm/s)	0.55	0.36
ΔE_Q (mm/s)	−1.0	−1.0
η	0.50	1.0

[a] For simplicity, isotropic A values were used in the simulation, even though an anisotropy less than 20% cannot be ruled out from the data.

Discussion

Using the rapid freeze-quench technique,[58,59] we have trapped and identified a kinetically competent intermediate in reconstitution of the native R2 subunit of *E. coli* RNR from apo R2, Fe^{2+}, and O_2. In the following paper,[42] we present kinetic data suggesting that this intermediate is the immediate precursor to the tyrosyl radical–diiron(III) cofactor, which is essential for RNR enzyme activity. The fact that a stoichiometry quantity of this iron intermediate can be generated in the mutant protein, R2-Y122F, has allowed for its detailed characterization by Mössbauer spectroscopy. Two distinct iron sites with antiparallel spins are detected. Their Mössbauer parameters (the values of the isomer shifts, the relatively small ΔE_Q, and the isotropic A values) are characteristic of high-spin ferric ions ($S = {}^5/_2$).[60]

In our previous report, we noted that two high-spin ferric ions cannot by themselves couple to form the observed system spin (S) of ${}^1/_2$ and proposed that a free radical was coupled to the two iron sites (thus, the designation "diferric radical intermediate").[38] Even though the magnetic hyperfine coupling constants, A, for the two iron sites are isotropic, a feature unique to high-spin ferric species, we thought it important to examine whether the magnitudes and opposite signs of the observed A values are consistent with the proposed structure. For this purpose, we have used a simple three-spin coupling model commonly applied to iron clusters.[61–63] In this model, three spins, $S_1 = S_2 = {}^5/_2$ for the two iron sites and $S_3 = {}^1/_2$ for the radical, were coupled to form the system spin $S = {}^1/_2$. Since the differing A values observed for the two iron sites indicate asymmetric coupling between the radical and the iron sites, we first coupled S_2 and S_3 to form an intermediate spin S_{23} and then coupled S_{23} and S_1 to form the final state. With the given S_1, S_2, and S_3, there are two different configurations for $S = {}^1/_2$. Using the conventional ket representation $|S_{23}; S\ M\rangle$, these two configurations can be represented as $|2; {}^1/_2\ {}^1/_2\rangle$ and $|3; {}^1/_2\ {}^1/_2\rangle$. The general state for $S = {}^1/_2$ and $M = {}^1/_2$ is therefore a quantum admixture of these two configurations:

$$|+\rangle = \sqrt{1-\alpha^2}\,|2; {}^1/_2\ {}^1/_2\rangle - \alpha|3; {}^1/_2\ {}^1/_2\rangle \quad (2)$$

(58) Bray, R. C. *Biochem. J.* **1961**, *81*, 189.
(59) Ballou, D. P.; Palmer, G. *Anal. Chem.* **1974**, *46*, 1248.
(60) Huynh, B. H.; Kent, T. A. *Adv. Inorg. Biochem.* **1984**, *6*, 163–223.
(61) Macedo, A. L.; Moura, I.; Moura, J. J. G.; LeGall, J.; Huynh, B. H. *Inorg. Chem.* **1993**, *32*, 1101–1105.
(62) Banci, L.; Betini, I.; Briganti, F. *New J. Chem.* **1991**, *15*, 467–477.
(63) Kent, T. A.; Huynh, B. H.; Münck, E. *Proc. Natl. Acad. Sci. U.S.A.* **1980**, *77*, 6574–6576.

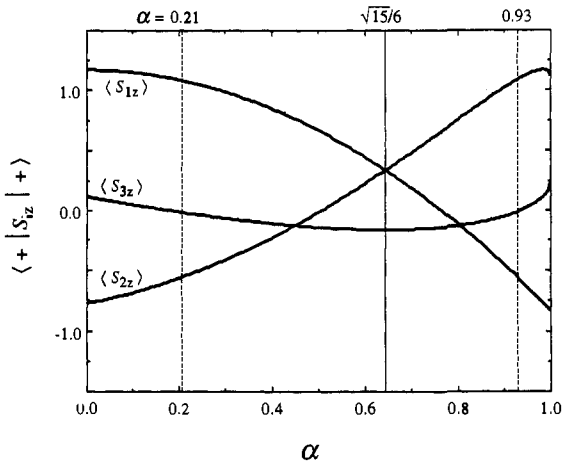

Figure 5. Plot of the expectation values $\langle +|S_{iz}|+\rangle$ as functions of the mixing coefficient α. The vertical line at $\alpha = \sqrt{15/6}$ separates the two regions containing equivalent solutions. The two dotted vertical lines are plotted at the positions $\alpha = 0.21$ and 0.93, illustrating that the same set of expectation values, which yield the observed A values, are obtained for these two α values.

where α is the mixing coefficient, $-1 \le \alpha \le +1$. For the ith site of the spin-coupled system, the observed magnetic hyperfine coupling constant A_i is related to its intrinsic coupling constant a_i by the following relation[61-63]

$$A_i = 2a_i\langle +|S_{iz}|+\rangle \qquad (3)$$

where $i = 1, 2,$ or 3. By using eq 2, the expectation value $\langle +|S_{iz}|+\rangle$ can be derived and expressed in terms of α.

$$\langle +|S_{1z}|+\rangle = {}^7/_6 - 2\alpha^2$$

$$\langle +|S_{2z}|+\rangle = {}^1/_9[17\alpha^2 + \sqrt{35}\alpha\sqrt{1-\alpha^2} - 7] \qquad (4)$$

$$\langle +|S_{3z}|+\rangle = {}^1/_9[\alpha^2 - \sqrt{35}\alpha\sqrt{1-\alpha^2} + 1]$$

With eqs 3 and 4, the observed A values can be calculated if the intrinsic a value is known. For high-spin ferric compounds, the intrinsic a value is dominated by the isotropic Fermi contact effect, which has been theoretically estimated [64] and experimentally verified[65,66] to be on the order of $(-22\text{ T})\times(g_n\beta_n)$. Depending on the coordination number and degree of covalency, a varies from $(-16\text{ T})\times(g_n\beta_n)$ for tetrahedral sulfur coordinated rubredoxin[67] to $(-22\text{ T})\times(g_n\beta_n)$ for Fe–tetraphenylporphyrin model compounds.[68] By using the theoretical a value for high-spin Fe(III), $(-22\text{ T})\times(g_n\beta_n)$ (which was found to be a good approximation for μ-oxo-bridged diiron clusters[66]), a value of the mixing coefficient α was sought that could reproduce the observed A values for the iron sites. In Figure 5, the expectation values, $\langle +|S_{iz}|+\rangle$, are plotted as functions of α.[69] From this plot it is obvious that only the region $0 \le \alpha \le \sqrt{15/6}$ must be searched: for each α value greater than $\sqrt{15/6}$, there exists a corresponding α between 0 and $\sqrt{15/6}$ which yields the same set of expectation values of S_{iz}, if the labels 1 and 2 are interchanged. For $\alpha = 0.21$ and $a = (-22\text{ T})\times(g_n\beta_n)$, eqs 3 and 4 yield theoretical A values for iron sites 1 and 2 ($A_1/(g_n\beta_n) = -48$ T and $A_2/(g_n\beta_n) = +25$ T) that are consistent (within 10%) with the observed values.

Thus, the magnetic properties of the diferric radical species can be explained by a simple three-spin coupling model which is consistent with our proposed structure. The model contains only a single parameter, namely, the mixing coefficient α, and it predicts correctly both the signs and magnitudes of the observed magnetic hyperfine coupling constants for the two iron sites. Moreover, this model suggests that the intrinsic a values for the iron sites are characteristic of high-spin Fe(III). It also provides insight concerning the spin-coupling nature of this diferric radical intermediate. The value 0.21 obtained for the mixing coefficient indicates that the ground state is predominantly (~96%) the state $|2; {}^1/_2\,{}^1/_2\rangle$. In other words, the spin-coupling nature of the diferric radical species may be described as follows: The free radical is antiferromagnetically coupled to the high-spin ferric ion with the positive A value (site 2) giving rise to an intermediate spin of 2, which is antiferromagnetically coupled to the iron site with the negative A value (site 1) resulting in an $S = {}^1/_2$ spin for the entire system. Interestingly, as mentioned above, for each value of α between 0 and $\sqrt{15/6}$, there exists an equivalent solution for $\alpha > \sqrt{15/6}$. For $\alpha = 0.21$, the equivalent solution has $\alpha = 0.93$. (See Figure 5. Please note that the expectation values of S_{1z} and S_{2z} are interchanged for these two solutions.) According to eq 2, this solution is predominantly (~85%) the state $|3; {}^1/_2\,{}^1/_2\rangle$. Consequently, the diferric radical species can also be described as a system consisting of a radical ferromagnetically coupled to the Fe site with the negative A value forming an intermediate spin of 3, which is antiferromagnetically coupled to the iron with the positive A value. In both descriptions, the key feature is that the spin of the radical is parallel to that of the negative-A-value Fe site and antiparallel to that of the positive-A-value iron site.

In addition to the magnitude and isotropy of the measured A-values, the ferric nature of the two iron sites in X is also indicated by their isomer shifts (δ). In general, δ varies with oxidation state, and follows the sequence $\delta_{Fe(IV)} < \delta_{Fe(III)} < \delta_{Fe(II)}$. Also, for the same oxidation state and ligand type, δ decreases with coordination number, $\delta_{tetrahedral} < \delta_{octahedral}$.[70] In the case of high-spin Fe(III) with oxygen-rich coordination, δ varies from 0.18 mm/s (room temperature[71]) for the tetrahedrally coordinated Fe(III) in solid $CaBaFe_4O_8$[72] to 0.55 mm/s for one of the ferric ions of the diferric cluster in *E. coli* RNR.[8,17] The isomer shifts determined for the diferric radical intermediate (0.55 mm/s for site 1 and 0.36 mm/s for site 2) fall within the range for high-spin ferric compounds. Most interestingly, δ for site 1 is at the high end of the range and identical with that of one of the iron sites in the product diferric cluster. Conversely, δ for site 2 is significantly less than the smaller δ for the diferric cluster (0.45 mm/s[8,17]). These data, along with the extensive structural information which is available for the iron cluster of R2,[5,6,73,74] permit some informed speculation concerning the structure of the diferric radical species.

Two obvious questions regarding the structure of the intermediate are the identity of the radical component and its spatial relationship to the Fe(III) ions. The spectroscopic data are consistent with a model in which the paramagnetic components

(64) Watson, R. E.; Freeman, A. J. *Phys. Rev.* **1961**, *123*, 2027.
(65) Oosterhuis, W. T.; Lang, G. *Phys. Rev.* **1969**, *178*, 439–456.
(66) Debrunner, P. G. *Hyperfine Interact.* **1990**, *53*, 21–36.
(67) Schulz, C. E.; Debrunner, P. G. *J. Phys. (Paris)* **1976**, *37* (*C6*), 154–158.
(68) Mashiko, T.; Kastner, M. E.; Spartalian, K.; Scheidt, W. R.; Reed, C. A. *J. Am. Chem. Soc.* **1978**, *100*, 6354–6362.
(69) There exists no solution for the region $-1 \le \alpha \le 0$. This region is therefore not shown.
(70) Greenwood, N. N.; Gibb, T. C. *Mössbauer Spectroscopy*; Chapman and Hall, Ltd.: London, 1971.
(71) Isomer shift decreases with increasing temperature due to the second-order Doppler effect. To compare with the 4.2 K values reported throughout this paper, approximately 0.09 mm/s should be added to this room temperature value.
(72) Ravi, N.; Jagannathan, R. J. *Phys. Chem. Solids* **1980**, *41*, 501–506.
(73) Regnström, K.; Aberg, A.; Ormö, M.; Sahlin, M., Sjöberg, B.-M. *J. Biol. Chem.* **1994**, *269*, 6355–6361.
(74) Aberg, A. Ph.D. Thesis, Stockholm University, 1993. This X-ray crystallographic study was carried out on a mutant R2 subunit, R2-S211A. The effect of this substitution on the structure of the diferruos cluster is not known, but it is expected to be minor.

are strongly coupled and therefore suggest that the radical is directly ligated to one or both of the Fe(III) ions. Thus, the radical is most likely derived from O_2 or from a ligand of either the diferrous or diferric cluster. The ligand arrangements about both oxidation states (diferrous and diferric) of the cluster are known from recent X-ray crystallographic experiments.[5,6,73,74] As illustrated in Figure 1, the ions of the diferric cluster are bridged (at an Fe–Fe distance of 3.3 Å) by the carboxylate group of E115 and by an oxo ligand, which recent resonance Raman experiments have shown to be derived from O_2.[53] Each iron coordinates a histidine and a water ligand. The two remaining ligands in the nearly octahedral coordination sphere of Fe_B[7] are glutamate carboxylate groups bound in monodentate fashion, while a single aspartate carboxylate (D84) is coordinated in bidentate fashion by Fe_A. The small bite angle of the bidentate D84 causes Fe_A to exhibit "a coordination with both trigonal bipyramidal and octahedral features."[5] Implications of this unusual coordination with respect to the Mössbauer parameters of the differic cluster and of the diferric radical species are discussed below.

The ions of the diferrous cluster[73,74] are 3.8 Å apart and, as in the diferric form, are bridged by E115. In contrast to the diferric cluster, no oxo bridge is present, but an additional carboxylate from E238 bridges the sites. In addition, the OH^- or H_2O ligand to Fe_A of the diferric cluster appears to be absent in the diferrous state, and D84 is only monodentate. Thus Fe_A is only 4-coordinate in the diferrous state, while Fe_B is 5-coordinate.[75] The crystallographic data thus indicate that the cofactor assembly reaction involves significant ligand reorganization about the iron cluster: insertion of an O_2-derived oxo bridge between the Fe ions, addition of an OH^- or H_2O ligand (which could be derived from either O_2 or H_2O) to Fe_A, and "carboxylate shifts"[76] by D84 (from monodentate to bidentate at Fe_A) and E238 (from bridging to monodentate at Fe_B).

On the basis of the unusual coordination of Fe_A, it is likely that this site is associated with the smaller δ (0.45 mm/s) and larger ΔE_Q (2.4 mm/s) of those observed[8,17] for the diferric cluster. Conversely, Fe_B probably exhibits the larger δ (0.55 mm/s) and smaller ΔE_Q (1.6 mm/s). It is intriguing to note that Fe site 1 of the diferric radical species has parameters (δ = 0.55 mm/s, ΔE_Q = 0.5–1.6 mm/s) which are quite similar to those which we have tentatively assigned to Fe_B of the diferric cluster. Likewise, δ for Fe site 2 of *X* is closer to, but significantly less than, the δ which we have assigned to Fe_A of the diferric cluster. It is tempting to speculate that Fe site 1 of the diferric radical species becomes Fe_B of the diferric cluster. The relatively small changes in its Mössbauer parameters might indicate that this Fe site undergoes relatively minor structural/electronic alterations during the conversion. By the same logic, Fe site 2, which we propose becomes Fe_A, may undergo more extensive rearrangements which cause its δ to increase from 0.36 to 0.45 mm/s and its ΔE_Q to increase to 2.4 mm/s. Several possibilities exist for the nature of this rearrangement. Increasing coordination number upon conversion to the diferric cluster might lead to an increase in δ. The carboxylate shift of D84 from monodentate to bidentate, formation of the Fe_A–OH_2 (or Fe_A–OH^-) bond, or formation of the Fe_A–oxo bond are all possibilities for increasing the coordination number of site 2 (Fe_A). Alternatively (or in addition) to increasing coordination, reduction of an electrophilic ligand might cause the observed changes. If the radical component of *X* were ligated to site 2 (Fe_A), reduction of this strongly electron withdrawing substituent upon conversion to the diferric cluster might explain the increase of δ of this site. In this scenario, the relatively small changes in the parameters of site 1 (Fe_B) might suggest that the radical is ligated exclusively to site 2 (Fe_A). It is gratifying to note that Fe_A is close to Y122 (~5.3 Å from the phenolic O).[5,6] Thus, ligation to site 2 (Fe_A) would position the radical component to oxidize Y122.

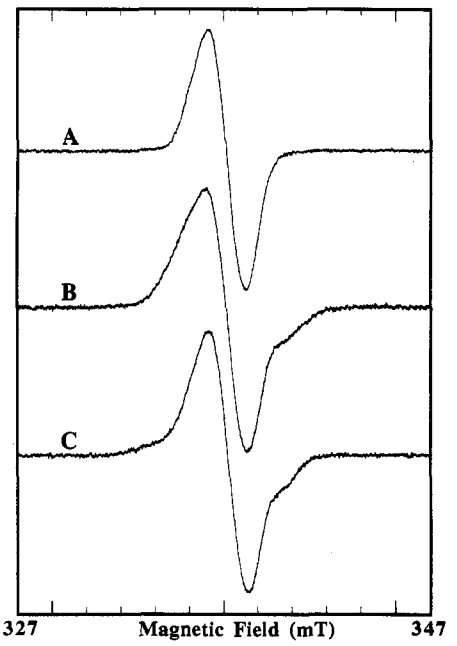

Figure 6. EPR spectra of the diferric radical species showing hyperfine coupling of ^{17}O from O_2 (B) and H_2O (C). The intermediate was generated by mixing equal volumes of oxygen-free apo R2-Y122F (0.14 mM) and an Fe^{2+} solution (1.0 mM) equilibrated (A) in air or (B) in ^{17}O-enriched O_2 gas (37% enrichment). Both reactions were quenched at 0.27 s. In part C, the reactant concentrations were the same, but both stock solutions were made up in ^{17}O-enriched (~32%) H_2O, both were air-saturated, and the reaction was quenched at 0.22 s. All spectra were recorded at 20 K with a microwave power of 6.7 μW, a modulation field of 0.4 mT, and a receiver gain of 10^5.

In spite of the above analysis, we cannot yet distinguish among ligation of the radical to Fe site 1, to site 2, or to both sites. Considering all the Fe ligands, possible candidates for the radical component include a carboxylyl radical derived from a D or E ligand, an imidazolyl radical derived from an H ligand, or an oxyl ($^{\bullet}O^-$) or hydroxyl radical ($^{\bullet}OH$) derived from O_2 or H_2O. Cyclic voltammetric studies indicate that, of the 20 common amino acids, the aromatic (H, Y, W) and sulfur-containing (C, M) residues are most easily oxidized.[77] These results provide argument against a carboxylyl radical, but do not allow a distinction to be made between an imidazolyl radical and an H_2O- or O_2-derived species. It is interesting to note that with α = 0.21 or 0.93, the expectation value ($+|S_{3z}|+$) for the radical is estimated to be –0.018. If the radical is assumed to be $^{\bullet}O^-$[78] this expectation value predicts an observed magnetic hyperfine interaction of $A/g_e\beta$ = ~0.2 mT in EPR for ^{17}O substitution. (For $^{17}{}^{\bullet}O^-$, the magnetic hyperfine interaction is axially symmetric with $(a_\parallel)/g_e\beta \approx$ 8–10 mT and $(a_\perp)g_e\beta \approx 2$ mT[79,80] as experienced by the electron[81]). The EPR spectra of the diferric radical species generated in the presence of $^{17}O_2$ (Figure 6B) or $H_2{}^{17}O$ (Figure 6C) exhibit hyperfine interactions similar in magnitude to this predicted value (compare

(75) Circular dichroism and magnetic circular dichroism studies correctly predicted that the ferrous ions of the diferrous cluster have coordination numbers less than six. Reem, R. C.; Foroughi, J.; Bollinger, J. M., Jr.; Jensen, G. M.; Stephens, P. J.; Stubbe, J.; Solomon, E. I. *New J. Chem.* **1991**, *15*, 439–444.

(76) Rardin, R. L.; Tolman, W. B.; Lippard, S. J. *New J. Chem.* **1991**, *15*, 417–430.

(77) Brabec, V.; Mornstein, V. *Biophys. Chem.* **1980**, *12*, 159–165.

(78) The possibility that the radical component of *X* is $^{\bullet}O^-$ raises the question of whether a distinction between Fe(III)–O– and Fe(IV)=O is merely semantic. As demonstrated below, the observed Mössbauer and EPR properties are consistent with the former configuration and incompatible with the latter.

(79) Wong, N. B.; Lunsford, J. H. *J. Chem. Phys.* **1971**, *55*, 3007–3012.

(80) Brailsford, J. R.; Morton, J. R.; Vannotti, L. E. *J. Chem. Phys.* **1968**, *49*, 2237–2240.

(81) In an EPR measurement, the magnetic hyperfine term $A/g_e\beta$ represents the magnetic field experienced by the electron, where g_e is the free electron *g*-value and β is the Bohr magneton, which is approximately 2000 times larger than the nuclear magneton, β_n.

to Figure 6A). Unfortunately, due to the low ^{17}O enrichment (37% in B and ~32% in C) and the poor resolution of the spectra, detailed analysis of these EPR data has not been successfully completed. Thus, identifying the radical component will require additional experiments.

Although the data presented above provide strong support for the diferric radical formulation of *X*, other investigators have suggested by analogy with the heme-iron peroxidases that the generation of •Y122 by the diiron cluster in RNR-R2 may involve one or more high-valent iron–oxo intermediates.[50-53,82] We have therefore considered the compatibility of the Mössbauer data with the presence of Fe(IV) in *X*. The spectral component of iron site 1 is very well resolved, and there exists no ambiguity that it originates from a high-spin ferric ion. In order to form the observed $S = {}^1/_2$ intermediate, the putative ferry ion would have to be high-spin Fe(IV) ($S = 2$). In general, Fe(IV) species (detected in iron oxides or in heme peroxidases) are low spin ($S = 1$) and exhibit characteristically small δ values between 0.0 and 0.15 mm/s.[66,70] A recently characterized non-heme high-spin Fe(IV) model compound also exhibits a characteristic δ of –0.03 mm/s.[83,84] In order to explore the possibility that iron site 2 may represent an Fe(IV) ion, we attempted to fit the spectral component of iron site 2 using $\delta = 0.0$ mm/s. With constraints set by the well-resolved low-energy line of iron site 2 and with δ set at 0.0 mm/s, the predicted total magnetic hyperfine splitting is too small and incompatible with the data. Recently, a transient iron species has been identified in methane monooxygenase during the interaction of O_2 with the diferrous hydroxylase.[85] This intermediate is characterized by a Mössbauer quadrupole doublet with $\Delta E_Q = 0.53$ mm/s and $\delta = 0.17$ mm/s. Although this value of δ is greater than those of previously characterized heme and non-heme Fe(IV) complexes,[66,70,83,84] the doublet was assigned to a diferryl cluster.[85] We therefore also explored the compatibility of the Mössbauer data with $\delta = 0.2$ mm/s for site 2 of *X*. By allowing anisotropic *A*-values, which are expected for high-spin Fe(IV) species, it is possible to obtain a set of parameters that yields a theoretical spectrum consistent with experimental spectra recorded in parallel applied field. This parameter set is incompatible, however, with the experimental spectrum recorded with perpendicular field (the spectrum shown in Figure 3B). In perpendicular field the $\Delta I_m = 0$ absorption lines, which are not seen in the parallel field spectra, acquire maximum intensity. With constraints set by the well-resolved low-energy line and with δ set at 0.2 mm/s, the low-energy $\Delta I_m = 0$ absorption line is fixed at –1.3 mm/s. No feature is observed at this velocity in the perpendicular field spectrum.

Additional evidence against an Fe(IV)–Fe(III) cluster designation for the intermediate is the observed (nearly) isotropic EPR signal at $g = 2.0$ ($g_\parallel = 2.006$, $g_\perp = 1.994$).[37,38] For a system consisting of a high-spin Fe(III) ($S = {}^5/_2$) coupled to a high-spin Fe(IV) ($S = 2$) forming a resultant $S = {}^1/_2$ spin, the system *g* tensor can be expressed in terms of the uncoupled intrinsic *g* tensors,

$$g = {}^7/_3 g_{Fe(III)} - {}^4/_3 g_{Fe(IV)} \quad (5)$$

Although the *g* tensor of high-spin Fe(IV) has not been well characterized, it is expected to exhibit considerable anisotropy, since the ground electronic state ^5D of high-spin Fe(IV) is identical with that of high-spin Fe(II), which exhibits a well-established anisotropic *g* tensor. The aforementioned study of a non-heme high-spin Fe(IV) model compound suggests an anisotropy of $\Delta g = 0.05$ and an average *g* value of 1.84.[84] By using these values in eq 5, one would predict an average *g* value for a Fe(IV)–Fe(III) cluster of 2.21, which is much greater than that observed for *X*, and an anisotropy approximately five times that observed for *X*. On the other hand, the three-spin coupling model proposed above yields a system *g* tensor dominated by the intrinsic high-spin ferric *g* tensors.

$$g = 2.161 g_{Fe(III)2} - 1.126 g_{Fe(III)1} - 0.035 g_{radical} \quad (6)$$

Since the contribution from the radical is small and the *g* tensor for high-spin ferric is generally isotropic and near the free electron value of 2.0, eq 6 yields a coupled *g* tensor consistent with the experimental data.

In summary, the Mössbauer and EPR data for *X* are consistent with the proposed diferric radical formulation of *X*, and inconsistent with an Fe(III), Fe(IV) formulation. Paper 2 in this series[42] presents kinetic data that are consistent with the proposal that *X* generates •Y122. Thus, for the cofactor assembly reaction carried out with excess Fe^{2+}, the data suggest that the •Y122-generating intermediate does not contain Fe(IV).

Acknowledgment. We thank Mr. Bud Puckett, the machinist extraordinaire in the Physics Department at Emory University, for his design and manufacture of the rapid freeze-quench Mössbauer sampling apparatus and for his effective solutions to our many technical and instrumental problems. We also thank Dr. Eckard Münck at Carnegie Mellon University for discussions on the coupling model for the diferric radical intermediate. This work was supported by NIH Grant GM 29595 to J.S. with a supplemental grant to D.E.E. and B.H.H. and by a Whitaker Health Sciences Foundation Fellowship to J.M.B.

(82) Lam, K.-Y.; Govindaraju, K.; Han, J.-Y.; Salmon, G. A.; Sykes, A. G. *J. Chem. Soc., Dalton Trans.* **1993**, 2797–2801.
(83) Collins, T. J.; Kostka, K. L.; Münck, E.; Uffelman, E. S. *J. Am. Chem. Soc.* **1990**, *112*, 5637–5639.
(84) Kostka, K. L.; Fox, B. G.; Hendrich, M. P.; Collins, T. J.; Rickard, C. E. F.; Wright, L. J.; Münck, E. *J. Am. Chem. Soc.* **1993**, *115*, 6746–6757.
(85) Lee, S.-K.; Fox, B. G.; Froland, W. A.; Lipscomb, J. D.; Münck, E. *J. Am. Chem. Soc.* **1993**, *115*, 6450–6451.
(86) Thelander, L. *J. Biol. Chem.* **1973**, *248*, 4591–4601.